https://doi.org/10.1093/cercor/bhae407 Advance access publication date 10 October 2024 Original Article

Functional specialization and distributed processing across marmoset lateral prefrontal subregions

Raymond Ka Wong (D^{1,2,*}, Janahan Selvanayagam (D^{1,2}, Kevin Johnston (D^{1,2,3}, Stefan Everling (D^{1,2,3}

- ¹Graduate Program in Neuroscience, University of Western Ontario, 1151 Richmond St, London, ON N6A 3K7, Canada
- ²Centre for Functional and Metabolic Mapping, Robarts Research Institute, University of Western Ontario, 1151 Richmond St, London, ON N6A 3K7, Canada
- ³Department of Physiology and Pharmacology, University of Western Ontario, 1151 Richmond St, London, ON N6A 3K7, Canada
- *Corresponding author: Raymond Ka Wong, Robarts Research Institute, University of Western Ontario, 1151 Richmond St, London, ON N6A 3K7, Canada. Email: raymond.ka.wong@hotmail.com

A prominent aspect of primate lateral prefrontal cortex organization is its division into several cytoarchitecturally distinct subregions. Neurophysiological investigations in macaques have provided evidence for the functional specialization of these subregions, but an understanding of the relative representational topography of sensory, social, and cognitive processes within them remains elusive. One explanatory factor is that evidence for functional specialization has been compiled largely from a patchwork of findings across studies, in many animals, and with considerable variation in stimulus sets and tasks. Here, we addressed this by leveraging the common marmoset (Callithrix jacchus) to carry out large-scale neurophysiological mapping of the lateral prefrontal cortex using high-density microelectrode arrays, and a diverse suite of test stimuli including faces, marmoset calls, and spatial working memory task. Task-modulated units and units responsive to visual and auditory stimuli were distributed throughout the lateral prefrontal cortex, while those with saccade-related activity or face-selective responses were restricted to 8aV, 8aD, 10, 46 V, and 47. Neurons with contralateral visual receptive fields were limited to areas 8aV and 8aD. These data reveal a mixed pattern of functional specialization in the lateral prefrontal cortex, in which responses to some stimuli and tasks are distributed broadly across lateral prefrontal cortex subregions, while others are more limited in their representation.

Key words: electrophysiology; marmoset; prefrontal cortex; working memory; visual; auditory; faces; vocalizations.

Introduction

The highly differentiated lateral prefrontal cortex (IPFC) in primates is involved in higher-order cognitive processes, including mental representation of abstract rules (Wallis et al. 2001; Everling and DeSouza 2005; Arnsten et al. 2012), working memory (Fuster and Alexander 1971), and executive control (Desimone and Duncan 1995; Miller and Cohen 2001). Neurons in this region also show responses to different stimulus modalities (visual, auditory), including complex stimuli such as faces and conspecific calls (O Scalaidhe et al. 1999; Romanski and Goldman-Rakic 2002; Sugihara et al. 2006; Romanski and Averbeck 2009; Riley et al. 2016; Haile et al. 2019). Studies of anatomical connectivity and cytoarchitecture show that the prefrontal cortex (PFC) is partitioned into numerous major cytoarchitectonic regions and even finer subdivisions by some parcellations (Barbas and Pandya 1989; Petrides 2005; Averbeck and Lee 2006; Sallet et al. 2013). It has also been proposed by O'Reilly (2010) that there is a systematic functional organization across IPFC areas, as functional architecture is a canonical property of the cerebral cortex (Van Essen and Glasser 2018). Addressing the functional parcellation of the lPFC is critical to our understanding of how the IPFC implements executive functions. As noted above, investigations in macaque IPFC have provided much insight into area-specific functionality, but our understanding is based primarily on area-specific parcellation and recordings across multiple animals and never spanning the entire IPFC in one animal. This potentially obscures some

functional differences as varying tasks and training protocols have been shown to affect both stimulus representations and their distribution within lPFC (Bichot et al. 1996; Rao et al. 1997).

A nonhuman primate species offering practical advantages for large-scale mapping of cortical areas is the small New World common marmoset (Callithrix jacchus). This species' relatively lissencephalic cortex also offers the opportunity for laminar electrophysiological recordings and optical imaging (Sadakane et al. 2015; Kondo et al. 2018; Johnston et al. 2019). Consequently, considerable effort has been directed toward an understanding of the cytoarchitectural differentiation of PFC subregions, and indeed, the marmoset IPFC is composed of a number of cytoarchitecturally distinct subfields believed to be homologous with those of macaques and humans (Burman et al. 2006; Reser et al. 2013). Despite the recent surge in popularity of the marmoset model (Mitchell and Leopold 2015; Okano 2021), the functions associated with these subregions are relatively poorly understood in this species and are an area of intensive investigation (Blum et al. 1982; Hung et al. 2015; Johnston et al. 2019; Liu et al. 2019; Selvanayagam et al. 2019; Schaeffer et al. 2019a; Schaeffer et al. 2019b; Schaeffer et al. 2020; Feizpour et al. 2021; Jovanovic et al. 2022; Wong et al. 2023). Given the well-established link between the lPFC and cognition, and the unique potential of the marmoset model for deriving an understanding of the cortical microcircuitry underlying aspects of social cognition such as vocal communication (Miller et al. 2016; Jovanovic et al. 2022; Samandra

et al. 2022; Grijseels et al. 2023), establishing a correspondence between the structural and functional organization of IPFC with respect to relatively simple tasks and social stimuli of multiple modalities is needed to provide an empirical foundation for interpretation of these more complex processes.

Here, we sought to characterize the response properties of single neurons in IPFC subregions using electrophysiological single-neuron recordings spanning a large portion of the IPFC within individual animals. Wireless extracellular electrophysiological recordings were obtained from head-unstrained or head-restrained animals (task-dependent), using a data-logging recording system from two adult marmosets with a 96-channel Utah array (4 \times 4 mm, 1.5 mm electrode length, 400 μ m pitch) implanted in the left lPFC, covering areas 8aV, 8aD, 9, 10, 46D, 46 V, and 47. To characterize these IPFC subregions, we recorded neural activity in response to a variety of visual and auditory stimuli and during the performance of a spatial working memory task.

Methods Subjects

Data were collected from two adult female common marmosets (C. jacchus; marmoset A, 26 months; marmoset B, 24 months). All experimental procedures conducted were in accordance with the Canadian Council of Animal Care policy on the care and use of laboratory animals and a protocol approved by the Animal Care Committee of the University of Western Ontario Council on Animal Care. The animals were under the close supervision of university veterinarians.

Array surgery

Animals underwent an aseptic surgical procedure under general anesthesia in which 96-channel electrode arrays (4 mm × 4 mm; 1.5 mm electrode length; 400 μ m pitch; iridium oxide tips) (Blackrock Neurotech, Salt Lake City, US) were implanted in the left PFC (see Selvanayagam et al. 2019 for details). During this surgery, a microdrill was used to perform a ~5 mm craniotomy, which was enlarged as necessary using a rongeur. The dura was removed, and the array was manually inserted into the lateral PFC; wires and connectors were fixed to the skull using dental adhesive and resin cement (All-Bond Universal and Duo-Link, Bisco Dental Products). Once implanted, the array site was covered with a thin layer of silicone adhesive (Kwik Sil; World Precision Instruments). A screw hole was drilled into the right side of the skull to place a stainlesssteel ground screw. The ground wire of the array was then tightly wound around the base of the screw to ensure a stable electrical connection. A combination recording chamber/head holder (Johnston et al. 2018) was placed around the array and connectors and fixed in place using further layers of dental adhesive and resin cement. Finally, a removable protective cap was placed on the chamber to protect the 3×32 -channel Omnetics connector.

Neural recordings

After recovery from array implantation, we verified that electrode contacts were within the cortex by monitoring extracellular neural activity using the SpikeGadgets' data acquisition system (SpikeGadgets, San Francisco, US). Upon observing single- or multiunit activity at multiple sites of the array for approximately 3 weeks, we commenced head-unrestrained or head-restrained (task-dependent) datalogger recordings of extracellular activity from the 96 implanted electrodes. A detailed description of these unrestrained datalogger-based recordings is presented in Wong et al. (2023). Initially, neural data underwent processing with a

common median filter to mitigate large movement-related artifacts. Subsequently, the data were further processed using a 4-pole Butterworth high-pass filter with a cutoff frequency of 500 Hz. Spike detection and sorting were then carried out offline using Plexon Offline Sorter v3. For our analysis, we included only those clearly isolated single units that exhibited baseline discharge rates exceeding 0.5 Hz. While offline sorting, we observed units drifting across time over the span of a session. In some cases where isolation was lost, these units were excluded from analysis.

We analyzed 3,482 neuronal recordings (20 sessions) from marmoset B and 2,482 neuronal recordings (14 sessions) from marmoset A. The number of neuronal recordings per session varied (marmoset B: 95 to 149 units; marmoset A: 60 to 150 units). A. It should be noted that the term "neuronal recordings" refers here to the total number of recorded units; however, these recordings may include repeated samplings of the same neurons across different sessions. This means that the actual number of unique neurons sampled is potentially less than the total number of recorded units reported. Thus, the figures provided represent the upper limit of the possible number of unique single units sampled across sessions. In line with this, it is important to acknowledge that these figures may overestimate the actual number of distinct neurons recorded, as they may reflect repeated measurements of the same neurons rather than distinct neuronal recordings.

Visual and auditory stimulus presentation and eye movement monitoring

For all visual receptive field mapping, visual stimulus presentation, and some auditory stimulus presentation sessions, we recorded neural activity while animals were head-restrained. In these sessions, marmosets were seated in a custom-designed primate chair (Johnston et al. 2018) inside a sound-attenuating chamber (Crist Instrument Co. Hagerstown MD), with the head restrained. A spout was placed at the animals' mouth to allow delivery of a viscous liquid reward (acacia gum) via an infusion pump (Model NE-510, New Era Pump Systems, Inc., Farmingdale, New York, USA). All visual stimuli were presented on a CRT monitor (ViewSonic Optiquest Q115, 76 Hz noninterlaced, 1,600 imes 1,280 resolution) using Monkeylogic (Hwang et al. 2019) on an ASUS UX430U Notebook PC running Windows 10. Eye positions were digitally recorded at 1 kHz via infrared video tracking of the left pupil (EyeLink 1000, SR Research, Ottawa, ON, Canada). Auditory stimulus presentation was controlled by Raspberry Pi 3 Model B and presented on a Bose Soundlink III speaker (Bose Corporation, Framingham, Mass.) connected to the audio output of the raspberry pi and placed at a distance of 10 cm centered in front of the animals and 12 cm below head level.

Experimental design and stimulus presentation Delayed-match-to-location task

Marmosets performed a delayed-match-to-location (DML) task on an in-house developed touchscreen testing box attached to the home cage (for details of touchscreen training protocol, see Wong et al. 2023). Each trial began with the presentation of a sample stimulus (filled blue or pink circle, 3 cm diameter) on a gray background at one of the four corner locations of the touchscreen display for a duration of 2.5 s. This was followed by a 2-s delay period in which the screen remained blank. After the delay period, choice stimuli (filled blue or pink circles, 3 cm diameter) were presented at each of the four corner locations, and the animal was required to touch the location matching the previously presented stimulus to obtain a liquid reward of 0.075 to 0.1 ml 50/50 mix of 1:1 acacia gum powder and water with liquid marshmallow. The reward was delivered via an infusion pump (model NE-510; New Era Pump Systems) through a liquid spout placed in front of the touchscreen monitor (Elo 1002 L). Trials were separated by 5 s intertrial periods.

Visual receptive field mapping

To map visual receptive fields in the IPFC of marmosets, we conducted a series of trials where a pseudorandom sequence of visual stimuli was displayed on the monitor. Each trial commenced with the animal fixating on a central dot for 500 ms. Following this initiation, circular stimuli, each subtending 0.2°, were presented rapidly at 9 pseudorandom locations selected from a pool of 48 possible sites (arranged in a 7×7 grid, covering $+/-12^{\circ}$ along both the ordinate and abscissa). Although eye position was monitored, animals were not required to maintain fixation during stimulus presentation. Stimulus onset asynchrony was set at 300 ms, with an interstimulus interval of 100 ms and an intertrial interval of 1 to 2 s. To sustain the alertness of the animals, a liquid reward was dispensed at the end of each trial.

Presentation of visual stimuli

To examine IPFC neuron responses to complex visual stimuli, we presented one of two distinct image sets in each recording session: (i) a collection of human and marmoset faces, scrambled faces, and objects, and (ii) images featuring arms, bodies, and faces of marmosets. In set 1, there were 6 human faces, 11 marmoset faces, 23 objects, and their corresponding scrambled versions (each stimulus presented roughly 19 times per session). The scrambling of faces involved dividing them into spatially segmented blocks and randomly shuffling these within and then across rows. Set 2 comprised 24 stimuli of each type (each presented about 14 times per session). All images subtended 3.5 degrees from the visual angle. During trials, the animals needed to fixate on a central dot (0.4°) for 300 to 500 ms before the display of a single image for 250 ms on the monitor. An intertrial interval of 2 s was maintained. Trials were aborted if the animal's gaze strayed beyond a 9° radius window centered on the displayed image.

Presentation of auditory stimuli

Acoustic stimuli of different conspecific calls (phee, trill, trillphee, twitter, chirp, ek, tsik, chatter) and scrambled (shuffled 25 ms windows over a 250 ms radius) versions of these calls were presented in three different contexts (head-restrained in a primate chair, head-unrestrained in a primate chair, and freely moving in their home cage) during each recording session. The order of context presentation was counterbalanced. In each context, the presentation of calls was pseudo-randomized with a 1 to 1.5-s intertrial interval. Stimuli were obtained in-house and from an open-source database (Landman et al. 2020). Our dataset consisted of eight different call types and two different calls for each call type. On average, each call was presented 48 times in each context and session. Calls were recorded in-house or obtained from an opensource database (Landman et al. 2020).

Data analysis

Analysis was performed using custom code written in Matlab (MathWorks) and Python. Statistical significance was evaluated at an alpha level of P < 0.02.

DML task

Previously published data from Wong et al. (2023) were included here. Activity within distinct nonoverlapping task epochs was assessed using analyses of variance (ANOVA) to compare the mean discharge rates of each neuron for each condition (four spatial locations) and each task epoch (baseline, sample, delay, preresponse, and postresponse). The baseline epoch was defined as the 1.5 s prior to the onset of the sample stimulus to the time of sample stimulus presentation. The sample epoch was defined as the 100 ms after the onset of the sample stimulus to the time of stimulus offset (2.4 s). We excluded the first 100 ms to avoid any potential sluggish sample-related activity contaminating estimates of delay-related activity. The delay epoch was 2 s in duration. The preresponse epoch was defined as the 300 ms period prior to the touch response, and the post-response epoch was defined as the 1,000 ms immediately after the touch response.

Visual receptive field mapping

ANOVAs were used to compare the mean discharge rates of each neuron for each task epoch (baseline, poststimulus) and condition (ipsilateral, contralateral). The baseline epoch was defined as the 200 ms prior to the trial onset for all stimulus presentations in that trial. The poststimulus epoch was 50 to 150 ms after stimulus onset. We excluded all stimulus presentations in which a saccade was made within ± -200 ms of stimulus onset.

Categorical visual stimuli

ANOVAs were used to compare the mean discharge rates of each neuron for each epoch (baseline, poststimulus) and condition (human face, marmoset face, scrambled faces, objects). The baseline epoch was defined as 450 ms prior to the stimulus onset to 50 ms after the stimulus onset. The peak response of a given neuron and its response to categorical images varied poststimulus presentation. To determine the peak response time, we calculated an average spike density function with a kernel filter that resembles a postsynaptic potential (Thompson et al. 1996) and determined the maximum peak or trough. Time constants for the growth and decay phases were set at 1 and 20 ms, respectively. The start and end of the poststimulus epoch for each neuron were then defined as the time at which the discharge rates reached 70% of the maximum response. A selectivity index for category and individual images were calculated as a contrast ratio using mean firing rates (FRs):

Category or Image with greatest mean FR — Category or Image with smallest mean FR Category or Image with greatest mean FR + Category or Image with smallest mean FR

Saccades

In sessions in which we presented visual stimuli of different categories, we analyzed the saccades made within each session. Blinks were excluded by excluding saccades that had an amplitude less than 0.5 and greater than 20 visual degrees, as well as a velocity greater than 1,200°. ANOVAs were used to compare the mean discharge rates of each neuron for each epoch (baseline, presaccadic, peri-saccadic, postsaccadic). The baseline epoch was defined as the 200 to 100 ms prior to saccade onset. The presaccadic epoch was 100 to 25 ms prior to saccade onset. The peri-saccadic epoch was 25 ms prior to saccade onset to 25 ms after saccade end. The post-saccadic epoch was 25 to 100 ms after saccade end.

Auditory responses

ANOVAs were used to compare the mean discharge rates of each neuron for each epoch (baseline, poststimulus), call type (phee, trill, trillphee, twitter, chirp, ek, tsik, chatter, scrambled), and context (head-restrained and head-unrestrained in a primate chair, freely moving in their home cage). The baseline epoch was defined

as the 200 ms prior to the stimulus onset to 50 ms after the stimulus onset. We noted that most neurons had an onset response to auditory stimuli that occurred at varying latencies and that the decay of this response varied across neurons and call types. To account for these variations in timing and response dynamics, accurately capture statistically these responses, and effectively allow a comparison between different call types, we constructed dynamic response epochs by aligning activity on stimulus onset and determining the times at which the observed poststimulus peak in activity reached 70% of the maximum discharge rate on both the rising and falling phases of the response. To determine the peak response time, we calculated an average spike density function with a kernel filter resembling a postsynaptic potential (Thompson et al. 1996) and found the maximum peak or trough. Time constants for the growth and decay phases were set at 1 and 20 ms, respectively. We then computed the mean discharge rate within this epoch, the beginning and end of which were delineated by these times. In practice, these resulting poststimulus epochs had a range of durations from 25 to 125 ms.

Natural grouping of neural discharge rates

We used an unsupervised clustering algorithm described by Kiani et al. (2015) to reveal potential spatially segregated clusters within the IPFC. For each recording session, we identified natural physiological groupings of recorded units based on the dissimilarity of their discharge rates (Kiani et al. 2015). The discharge rate dissimilarity reflects the covariation of neural discharge rates and can take any value between 0 (perfect correlation) and 2 (perfect anticorrelation). We defined the neural discharge rate vector for each unit in 30 ms nonoverlapping bins from the beginning to end of recording sessions, independent of task epochs and the animal's behavior. Dissimilarities for all possible pairs of units in a given session were calculated, and a 96 \times 96 dissimilarity matrix for all possible pairs of recording channels was created for each session. Dissimilarity matrixes across sessions were averaged for each animal separately.

We applied nonlinear multidimensional scaling (MDS) to the averaged dissimilarity matrix to create a low-dimensional representation that retained the pairwise relationships as much as possible. To explore the spatial relationship between recording channels, we chose a unique color for each recording channel based on its location in the 2D MDS map and a 2D color map. Locations on the array with similar colors represent natural physiological groupings of recorded units.

Array localization

Marmosets were euthanized at the end of the data acquisition process to prepare the brains for ex vivo magnetic resonance imaging (MRI) scans (Wong et al. 2023). The animals were deeply anesthetized with 20 mg/kg of ketamine plus 0.025 mg/kg medetomidine and 5% isoflurane in 1.4% to 2% oxygen to reach beyond the surgical plane (i.e. no response to toe pinching or cornea touching). They were then transcardially perfused with 0.9% sodium chloride irrigation solution, followed by 10% buffered formalin. The brain was then extracted and stored in 10% buffered formalin for more than a week before ex vivo MRI. On the day of the scan, the brain was transferred to another container for imaging and immersed in a fluorine-based lubricant (Christo-lube; Lubrication Technology) to improve homogeneity and avoid susceptibility artifacts at the boundaries. Ex vivo MRI was performed on a 9.4T 31 cm horizontal bore magnet (Varian/Agilent, Yarnton, UK) and Bruker BioSpec Avance III console with the software package Paravision-7 (Bruker BioSpin

Corp., Billerica, MA), a custom-built high-performance 15-cmdiameter gradient coil with 400 mT/m maximum gradient strength (xMR, London, CAN; Peterson et al. 2018), and an mp30 (Varian Inc., Palo Alto, USA) transmit/receive coil. High-resolution $(100 \times 100 \times 100 \,\mu\text{m})$ T2-weighted images were acquired for each animal. The raw MRI images were converted to NifTI format using dcm2niix (Li et al. 2016), and the MRIs were nonlinearly registered to the ultra-high-resolution ex vivo National Institutes of Health (NIH) template brain (Liu et al. 2018), which contains the location of cytoarchitectonic boundaries of the Paxinos atlas (Paxinos et al. 2012), using Advanced Normalization Tools (Avants et al. 2011) software. The resultant transformation matrices were then applied to the cytoarchitectonic boundary image included with the NIH template brain atlas. These cytoarchitectonic boundaries overlayed on the registered ex vivo anatomical T2 images were used to reconstruct the location of the implanted array in each marmoset. Images were rendered in 3D using the program MRIcroGL and overlayed the Paxinos atlas cytoarchitectural boundaries for estimating where the arrays were implanted in each animal (Fig. 1).

Results

Overall, neurons across many areas of marmoset PFC exhibited significant modulations in activity during a cognitive task as well as during presentations of visual and auditory stimuli and across differing experimental contexts. Single neuron examples depicting these modulations are presented in Fig. 2. As noted in our previously published work (Wong et al. 2023), we observed taskrelated activity during the sample, delay, and response epochs of the DML task, with many neurons exhibiting modulations in one or more of these epochs (Fig. 2A). We observed neurons with visual receptive fields (Fig. 2B). We noted that a range of visual stimuli including faces, objects, and body parts also evoked robust responses that were selective for the stimulus type in many cases (Fig. 2C). We additionally observed presaccadic and robust postsaccadic activity (Fig. 2D). Finally, we observed call-selective auditory responses in PFC neurons (Fig. 2E) that were in some cases modulated across experimental contexts including headrestrained, head-unrestrained, and within the home cage (Fig. 2E). Specific analyses investigating these responses are detailed below.

Neurons in most lPFC subregions respond during a working memory task

The relationship between the observed responses in all epochs of the DML task and the IPFC subregions in which they were recorded is shown in Fig. 3A, which presents the proportion of all units recorded at a given array location that were significantly modulated within each task epoch, pooled across all sessions in which the DML task was run. Overall, we found that single neurons exhibited significant modulations in all task epochs across all IPFC subregions but noted that the proportion of units with delay activity was relatively lower in areas 9 and 10. One possibility, noted also in earlier work (see Goldman-Rakic 1995), was that animals were able to correctly perform the task not by relying on WM per se, but rather by simply orienting the head or whole body toward the location of the stimulus during the sample presentation and maintaining that orientation throughout the delay period until responding. We addressed these by reviewing videos of all trials and excluded trials in which the animals fixated on the location of the sample, as well as examining the occurrence of same-side versus opposite-side errors. Detailed analyses of these data have been reported previously (Wong et al. 2023).

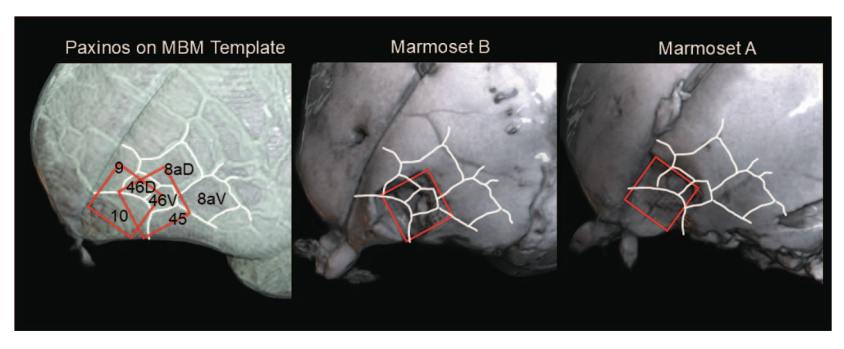


Fig. 1. Reconstruction of array implantation sites. T-2-weighted MRIs were acquired and nonlinearly registered to the NIH template brain that contains the location of cytoarchitectonic boundaries of the Paxinos atlas (see Methods). Images were rendered in 3D using MRIcroGL and overlayed with the Paxinos atlas cytoarchitectural boundaries on: the Marmoset Brain Template (left panel); marmoset B (middle panel); marmoset a (right panel).

PFC visual receptive fields were largely bilateral

We carried out separate two-way ANOVAs on discharge rates of IPFC neurons with factors of epoch (baseline-0 to 200 ms prior to stimulus onset, visual—50 to 150 ms following stimulus onset) and location (contralateral, ipsilateral), to determine rough estimates of lateralization of their visual receptive fields. Neurons exhibiting a significant interaction and/or a main effect of the epoch were considered visual. In marmoset B, 225/416 (54.1%) neurons were classified as visual, of which 34 and 6 neurons had contralateral and ipsilateral receptive fields, respectively. In marmoset A, 108/365 (37.0%) neurons were classified as visual, with 3 and 5 neurons having well-defined contralateral and ipsilateral receptive fields, respectively. Overall, most neurons with visual activity exhibited these responses across a broad range of locations encompassing both ipsi- and contralateral visual fields. The proportions of all recorded units exhibiting statistically significant visual responses and location-selective responses across IPFC subregions are depicted in Fig. 3B. We found units with visual activity at all locations at which we found well-isolated single units, with a notable cluster of neurons in 8aV that had contralateral receptive fields.

IPFC neurons respond to many categories of visual stimuli

In separate recording sessions, we presented marmosets with two distinct sets of categorical images. Set one included images of human faces, marmoset faces, scrambled faces, and objects. Set two comprised images of marmoset arms, bodies, and faces. To assess whether marmoset IPFC neurons responded to these categorical images, we performed two-way ANOVAs for both the baseline and poststimulus onset epochs. Neurons demonstrating a significant interaction and/or a main effect of the epoch were identified as visually responsive.

For the sessions presenting the first set of images, the response patterns were as follows: In marmoset B, 61.4% (234/381) of neurons showed visual activity, with 26.9% responsive to human faces, 18.8% to marmoset faces, and 31.2% to objects/scrambled images. In marmoset A, 37.0% (118/319) exhibited visual activity, with respective responsiveness of 33.1% to human faces, 33.1% to marmoset faces, and 39.8% to objects/scrambled images. Notably, neurons responsive to faces showed higher discharge rates for human faces than for marmoset faces (one-sample t-test: P < 0.001).

In sessions with the second set of images (marmoset arms, bodies, and faces), marmoset B had 68.2% (180/264) of neurons displaying visual activity, with 31.1% responding to faces and 25.6% to arms/bodies. In marmoset A, 37.2% (148/398) showed

visual activity, with 26.4% responsive to faces and 19.6% to arms/hodies

To quantify differences in activity between categories and individual images, we calculated a selectivity index. Supplementary Fig. 1 shows the averaged selectivity indices for all responsive neurons at each array location, revealing a tendency for marmoset PFC neurons to prefer individual images over specific categories. We observed visual activity across all locations with well-isolated single units (Fig. 3C and D) and noted clusters of face-selective neurons in areas 8aD, 10, and 47 (Fig. 3C and D).

Saccade-related responses in marmoset lPFC neurons

To determine whether marmoset IPFC neurons exhibited saccaderelated activity, we carried out separate one-way ANOVAs at each epoch (baseline, presaccadic, peri-saccadic, and postsaccadic). Neurons with a main effect were considered saccade-related. In marmoset B, 314/645 (48.7%) neurons were saccade-related, with 12.4% of neurons having presaccadic, 30.2% having peri-saccadic and 34.9% having postsaccadic activity. In marmoset A, 70/717 (9.8%) neurons were saccade-related, with 2.4%, 5.2%, and 7.0% of neurons having pre-, peri- and postsaccadic activity, respectively. In general, many PFC neurons had activity related to spontaneous saccades with a bias toward postsaccadic responses. Saccaderelated units were found to be distributed throughout the PFC, with clusters of neurons in areas 8aD, 8aV, 47, 46 V, and dorsal area 10 (Fig. 3E).

lPFC neurons are responsive to but not selective for conspecific calls

To determine whether marmoset PFC neurons exhibited responses to auditory stimuli consisting of conspecific calls, we carried out three-way mixed ANOVAs for the analysis of call-type (phee, twitter, trill, trillphee, chirp, ek, chatter, tsik, scrambled) at each epoch (before and after auditory stimuli) for each experimental context (head-restrained in chair, head-unrestrained in chair and head-unrestrained in home cage). Neurons with a significant interaction and/or a main effect of epoch were considered as having auditory responses.

In marmoset B, 191/373 (51.2%) neurons had auditory activity, 84 (22.5%) neurons had a three-way interaction, 46 (12.3%) neurons had an interaction between call type and epoch, 44 (11.7%) neurons had an interaction between context and epoch, and 41 (11.0%) neurons had a main effect of epoch. Of the 67 neurons that had an interaction of call type and epoch (including 21 which had a higher order interaction), 14 were responsive to one call type, 9 were responsive to two call types, 5 were responsive

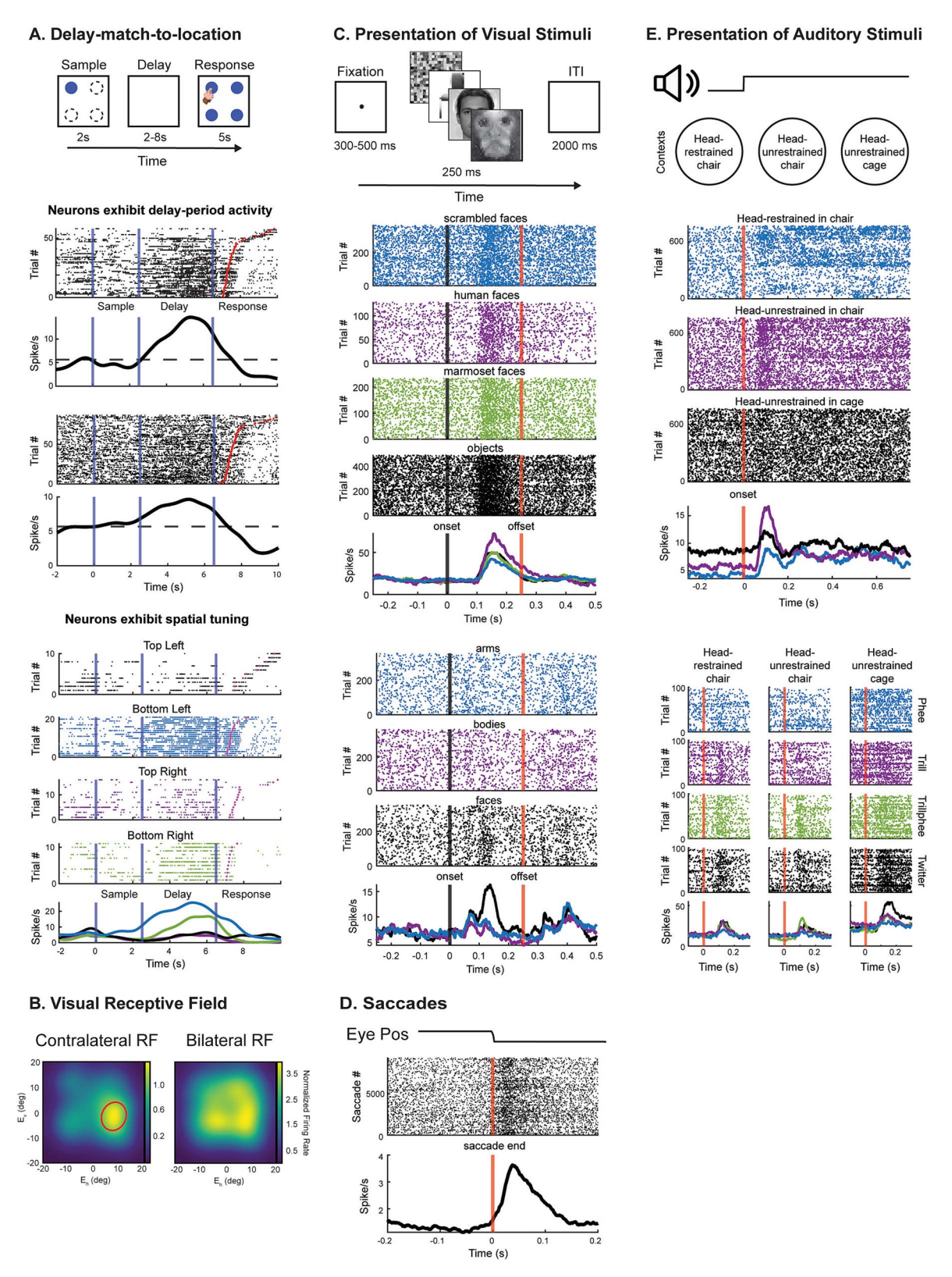


Fig. 2. Example single marmoset IPFC neurons modulated by task and stimulus. A) Top panel, task timeline. Rasters and spike density functions in the panels below depict single units exhibiting significant modulations in discharge rate during the delay epoch. Panels below depict a single neuron exhibiting spatial tuning. B) Example of neurons with contralateral and bilateral receptive fields. C) Top panel, task timeline. Below depicts a single neuron exhibiting visual response to all categories of images, but selectivity for human faces (visual stimuli set 1) and another neuron showing selectivity to faces compared to arms and bodies (visual stimuli set 2). D) Rasters and spike density functions of example neurons exhibiting presaccadic and postsaccadic activity. E) Top panel, task schematic. Middle panel depicts a single neuron's response in different contexts. Bottom panel shows a single neuron's response to different call types in different contexts.

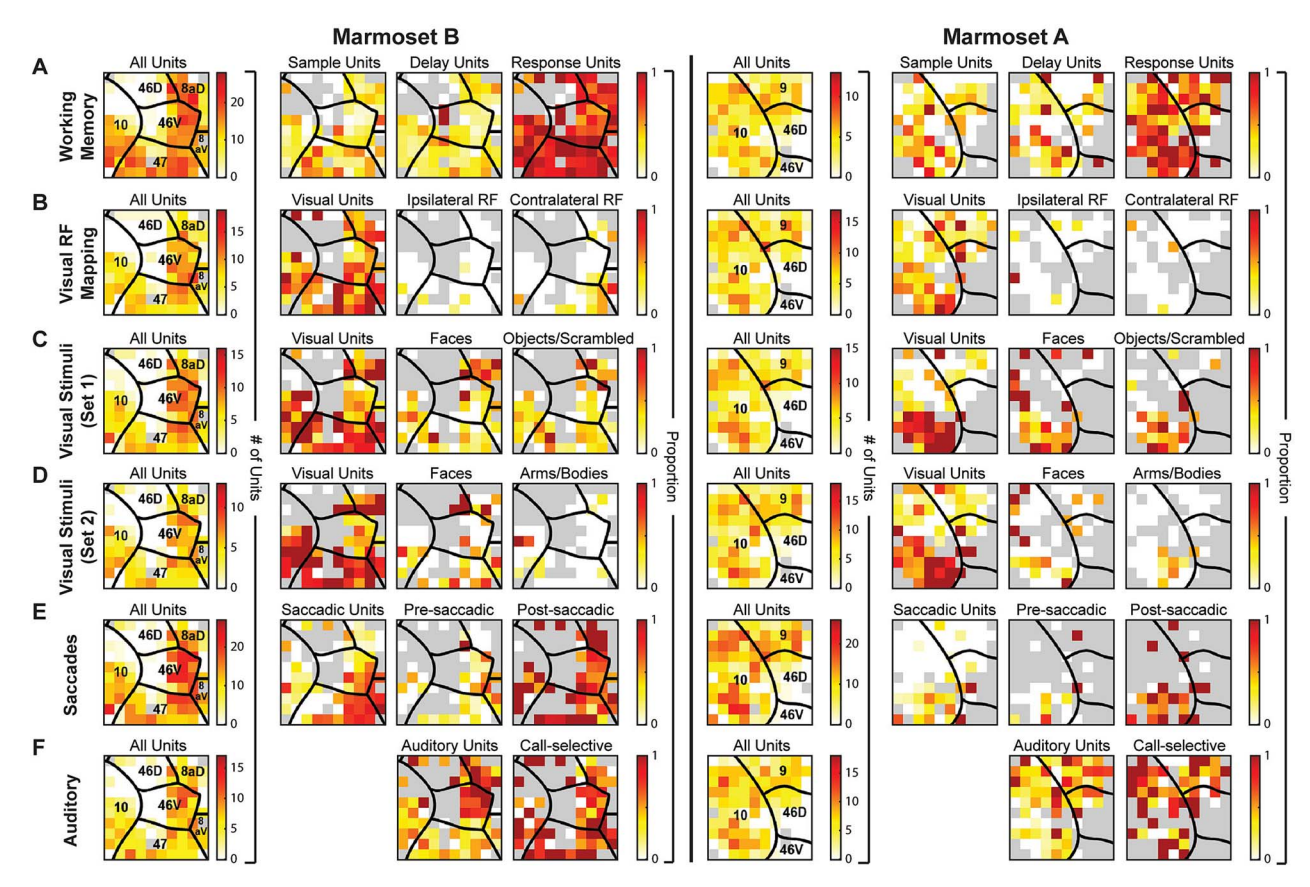


Fig. 3. Distribution of task-modulated units and units responsive to different stimulus modalities. Array locations were reconstructed using highresolution MRIs and superimposed on a standardized marmoset brain, area boundaries from Paxinos et al. (2012). The first column (left column) represents the total number of units found across sessions and its distribution on the array. Second column represents the proportion of units compared to the first column. The third and/or fourth column represents the proportion of units compared to the second column. Gray depicts array locations at which well-isolated single units were not observed.

to three call types and 39 were responsive to more than three call types (excluding scrambled). In marmoset A, 157/418 (37.6%) neurons had auditory activity: 65 (15.5%) neurons had a threeway interaction, 36 (8.6%) neurons had an interaction between call type and epoch, 17 (4.1%) neurons had an interaction between context and epoch, and 49 (11.7%) neurons had a main effect of epoch. Of the 51 neurons that had an interaction of call type and epoch (including 15 which had a higher order interaction), 13 were responsive to one call type, 16 were responsive to two call types, 7 were responsive to three call types and 15 were responsive to more than three call types (excluding scrambled).

In neurons with a 3-way interaction, we conducted Bonferroni corrected pairwise comparisons to examine differences in discharge activity from baseline for different call types in different contexts. In marmoset B, 45/84 (53.6%) of neurons with a 3-way interaction exhibited a response to at least one call type in only one context, 28/84 (33.3%) of neurons exhibited a response to at least one call type in two contexts, and 11/84 (13.1%) of neurons exhibited a response to at least one call type in all three contexts. In marmoset A, 37/65 (56.9%), 24/65 (36.9%) and 4/65 (6.2%) of neurons with a 3-way interaction exhibited a response to at least one call type in only one, two, and all three contexts, respectively. We observed no systematic effect of experimental context on responses to different call types; a neuron's response profile for calls in one context does not necessarily represent the same response profile for calls in another context. Altogether, we found that most call-responsive neurons exhibited responses to multiple call types in multiple contexts (see Fig. 2E, bottom panel).

Auditory and call-selective neurons were observed in multiple experimental contexts throughout all PFC subregions, with a higher proportion of auditory neurons in areas 8aD, 46D, and 9 and the dorsal portion of area 10 (Fig. 3F).

Population responses from neuron classes with different types of selectivity

To determine how variable the population activity is, we plotted the population responses from neuron classes (excited or suppressed; P < 0.02) with different types of selectivity for each task (Fig. 4). Firing rates are normalized, and the standard error is plotted in a lighter shade. Figure 4A shows the population responses of task-modulated activity during each epoch (sample, delay, preresponse, postresponse). Population responses to different visual stimuli are shown in Fig. 4B (Visual Stimuli Set 1) and Fig. 4C (Visual Stimuli Set 2). In general, neurons from the same class respond similarly to all categories of images. Figure 4D shows the population responses of presaccadic and postsaccadic neurons. From the subset of neurons that we recorded, 28.9% of presaccadic neurons (n = 28) were excited and 71.1% were suppressed (n = 69). On the contrary, 65.9% and 34.1% of postsaccadic neurons were excited and suppressed (n = 184 and 95), respectively. Population responses of auditory units to the preferred and nonpreferred stimulus of different neuron classes are shown in Fig. 4E. The magnitude of response for both classes of neurons is larger in response to the preferred stimulus than the nonpreferred stimulus. Overall, the variability between neuron classes with different

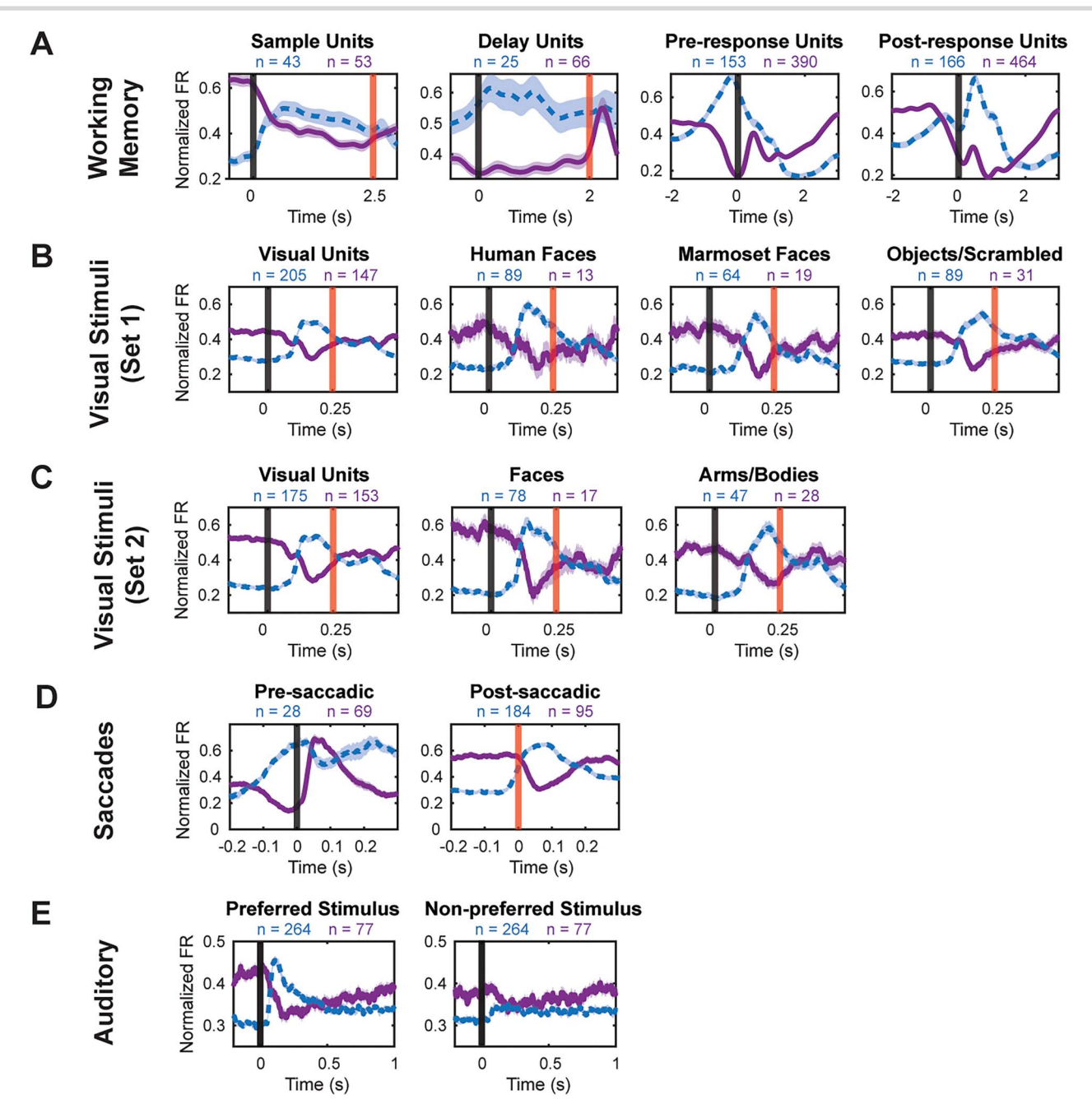


Fig. 4. Population responses from neuron classes with different types of selectivity. Dashed line represents neurons that exhibited an increased firing rate compared to baseline (P < 0.02; excitation), and the solid line represents neurons that exhibited a decreased firing rate compared to baseline (P < 0.02; suppression). Firing rates are normalized, and the standard error is plotted in a lighter shade. Vertical black lines represent the start of the epoch/event. Vertical red lines represent the end of the epoch/event. *n* represents the number of neurons.

types of selectivity is low, such that neurons classes with the same selectivity respond similarly.

Natural grouping of neural responses reveals spatially segregated clusters in marmoset lPFC

We used unsupervised algorithms (Kiani et al. 2015) to identify natural groupings of neurons based on their response covariation within recording sessions. With these objectively identified groupings of neurons, we projected back onto the arrays to determine whether neurons were spatially segregated in a topographic manner. Though IPFC regions may have similar response properties, this method can reveal a topography that is defined at the population level. Figure 5 shows the MDS-filtered dissimilarity

matrix color map in which similar colors depict neurons with similar responses. (see Natural Grouping of Neural Discharge Rates in Methods).

Based on this analysis, we found that the PFC was divided into functional subregions, similar to the cytoarchitectural boundaries we outlined, and potentially into further smaller subregions in area 10, dorsal and ventral. Overall, this indicates that although single PFC neurons across PFC subregions are responsive to many stimuli and modulated during a WM task (see summaries in Table 1 and Fig. 6), responses within a given subregion are more similar to each other than those across subregions. This is suggestive of a degree of functional localization in marmoset PFC.

Table 1. Summary of IPFC subregions within which task-modulated units and units responsive to varying stimulus modalities were found in marmosets A and B.

Modality	Prefrontal area						
	8aV	8aD	9	10	46D	46 V	47
Subject	В	В	A	A&B	A&B	A&B	В
WM: sample units	/	✓	✓	✓	✓	✓	/
WM: delay units	✓	✓	✓	✓	✓	✓	✓
WM: response units	✓	✓	✓	✓	✓	✓	/
Visual units	/	V	/	/	V	/	1
Contralateral Receptive	/	V					/
Field							
Faces	✓	✓		✓	✓	✓	/
Auditory units	1	/	✓	V	/	/	/
Call-selective units	/	V	/	/	V	/	1
Saccadic units	V	<i>\</i>	•	V	•	/	1

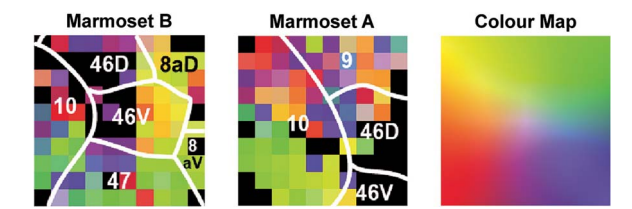


Fig. 5. Natural grouping of neural discharge rates reveals spatially segregated clusters. For each session, we identified natural physiological groupings of recorded units based on the dissimilarity of their discharge rates (see Methods). To create a low-dimensional representation and to explore the spatial relationship between recording channels, we chose a unique color for each recording channel based on its location in the 2D MDS map and a 2D color map (a spatial color map is used for the projection of unit colors onto recording electrodes). Locations on the array with similar colors represent natural physiological groupings of recorded units. The color map is provided to indicate which colors are closer to one another. Note: Similar colors between animals do not represent similar physiological groups.

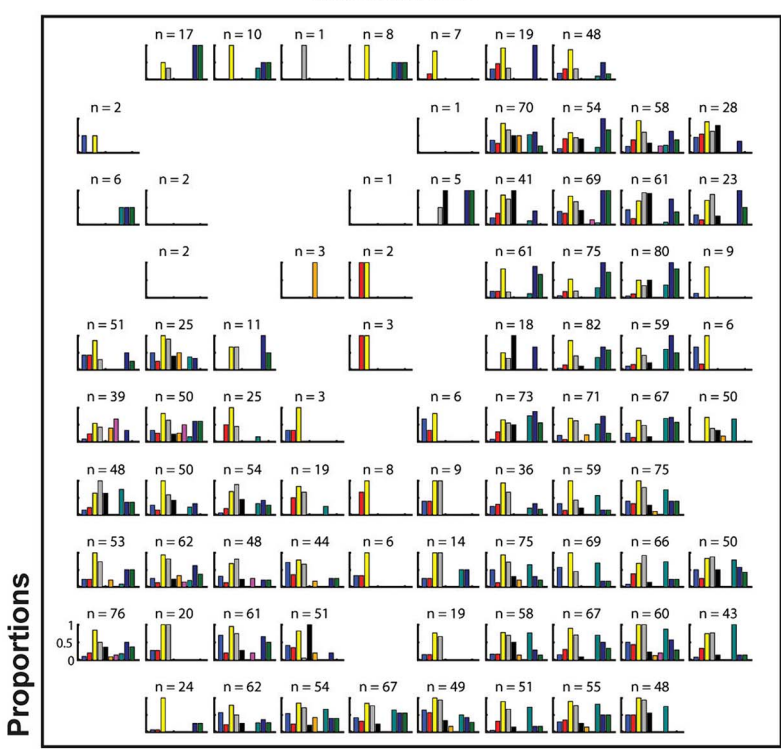
Discussion

The common marmoset is a model of growing popularity for studies of cognitive processes and has great potential as a model animal for investigations of the neural basis of social cognition (Samandra et al. 2022). The role of the PFC in cognitive processes and the specific roles of IPFC subregions have been investigated in myriad neurophysiological studies in rhesus macaques (Hoshi 2006; Wise 2008); however, far fewer studies have investigated the responses of marmoset lPFC neurons to social and nonsocial visual and auditory stimuli or during cognitive tasks. Here, we sought to characterize the responses of marmoset IPFC neurons across a suite of subregions by employing a broad test battery including a spatial working memory task, visual receptive field mapping task, the presentation of differing categories of social and nonsocial images, and social and nonsocial auditory stimuli. Task-modulated neurons and neurons responsive to different stimulus modalities were found throughout the IPFC of marmosets, with relatively subtle variations across recording locations and hence cytoarchitectonic boundaries (see summaries in Table 1 and Fig. 4). Interestingly, in spite of the broad distribution of responses to a widely varied suite of visual and auditory stimuli, we found that the recorded population of neurons in the PFC was not homogeneous but could be divided into smaller subregions with a clustering, similar to cytoarchitectural boundaries

based on task-independent covariation of neural responses. This suggests that the responsiveness of lPFC neurons across areal boundaries during many task epochs and to many stimuli is superimposed onto a basic pattern of greater discharge covariation within rather than between IPFC subregions. It is important to note that while we report 3,482 neuronal recordings from marmoset B and 2,482 from marmoset A, these numbers represent the upper limit of recorded units. Given the possibility that some neurons may have been sampled on multiple occasions across different sessions, the actual number of unique single units could be smaller. As such, caution should be exercised when interpreting these figures, as they may reflect repeated measurements of the same neurons rather than distinct neuronal recordings. This limitation underscores the need for further investigation into the stability and variability of neuronal recordings across sessions to gain a more accurate estimate of the number of distinct units involved in these tasks.

As we have reported previously (Wong et al. 2023), we observed activity in a spatial WM task in marmoset lPFC neurons that was remarkably similar to initial reports by Fuster and Kubota in the macaque (Fuster and Alexander 1971; Kubota and Niki 1971). Like macaque IPFC neurons, in the DML task, marmoset IPFC neurons exhibited sample-, delay-, and response-related activity. In the present data set, delay period activity seemed weaker and less spatially selective (Wong et al. 2023) than is typically observed in macaques. This may be in part attributable to several factors including differences between our touchscreen task and the oculomotor delayed response (ODR) task often used in studies of the neurophysiological basis of spatial WM in macaques: The spatial reference frame in our task was not retinocentric as in the ODR task; animals were free to move and orient during the delay period; our task did not require the animals to retain a finegrained representation of spatial locations since we used only four widely spaced and relatively large sample locations. We observed task-related activity in all subregions but noted that the proportion of units with delay-related activity was relatively lower in areas 9 and 10. Given the anatomical connections of these areas to temporal cortical areas associated with higher order auditory and visual stimuli (see Burman et al. 2006), and our observations here of predominantly auditory responses in these areas, consistent with previous anatomical work in marmoset area 10 (Burman et al. 2011), this finding suggests that these areas may not have a significant role in the short-term retention of visual information. Excitotoxic lesions of area 9 in marmosets have been shown to





Marmoset A

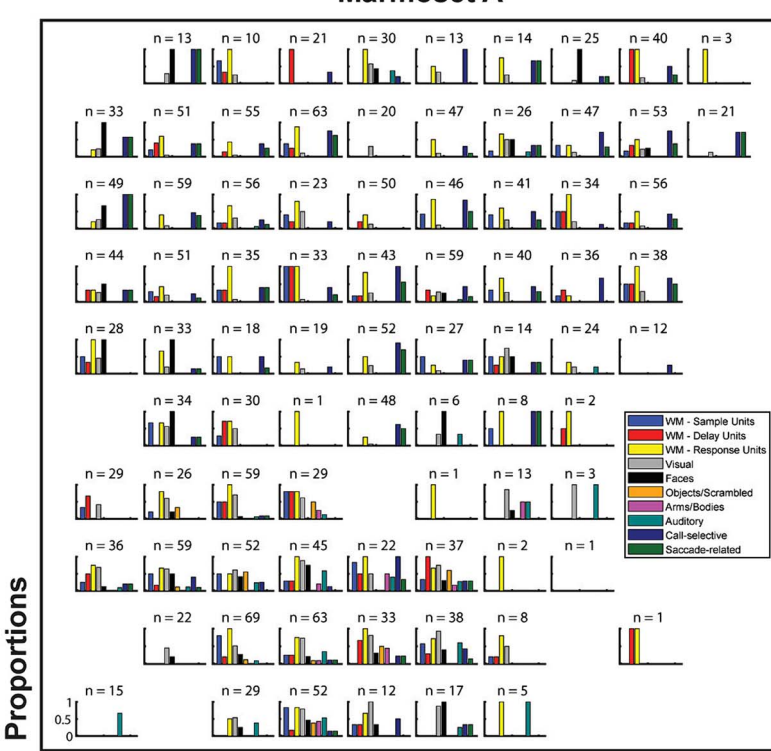


Fig. 6. Proportions of task-modulated units and units responsive to different stimulus modalities at each electrode contact in marmoset B A) and marmoset A B). n indicates the overall total number of units at each electrode contact. Proportions were not calculated with respect to the overall total number of units, but rather in respect to the total number of units found in task-specific sessions.

impair inhibitory control in a complex set-shifting task (Dias et al. 1996), suggesting that this area may be involved more in attentional shifting rather than retention. Similarly, lesions of area 10 in macaques have not been shown to result in impairments in WM (Mansouri et al. 2015), and single neuron recordings in this region have revealed not persistent activity but rather responses related to reward-based feedback of trial outcomes (Tsujimoto et al. 2010, 2012). This evidence suggests that, as in the case of area 9, this area is involved in the orchestration of behavioral shifts. Although further investigations comparing these types of tasks will be required to establish definitively the roles of areas 9 and 10 in cognitive processes, the practical advantages of the marmoset model with respect to freely moving and untethered recordings in naturalistic tasks offer intriguing possibilities of deriving a greater understanding of frontopolar areas in particular, which have only recently been investigated in the macaque and the cognitive functions of which remain relatively poorly understood (Mansouri et al. 2017).

In light of previous work establishing visual responses and visual receptive fields in IPFC neurons (Boch and Goldberg 1989) and the well-established role of IPFC in visual attention (Rossi et al. 2009), we investigated visual receptive fields of lPFC neurons. Consistent with a previous report that found robust visual responses in a broad region of PFC including areas 6DR, 8aD, 8aV, 8C, and 46 V (Feizpour et al. 2021), we observed units with visual responses in virtually all IPFC areas that we recorded, including areas 9, 10, and 46D, which were not sampled in that study due to the locations of their array implantations that also included areas 8C, 6Va, and 6 DC and importantly established visual responses in these areas as well. As in that study, we noted that the greatest proportion of visual units was found in area 8aV and that neurons in this area exhibited contralateral response fields. This, together with our finding of a large proportion of neurons with saccade-related activity in this area, is consistent with previous evidence suggesting that these areas contain the marmoset FEF (Selvanayagam et al. 2019; Feizpour et al. 2021).

During sessions in which marmosets were presented with visual stimuli belonging to different categories, neurons with visual responses were found in all IPFC subregions. We found clusters of face-selective neurons in areas 8aV, 8aD, 10, 46 V, and 47 but no specific topography for arms, bodies, objects, or scrambled images. A previous functional MRI (fMRI) study in awake marmosets observed activation in frontal areas, predominately 8aV and 45, for images of marmoset faces, bodies, objects, and scrambled versions of these images (Hung et al. 2015). In a subsequent fMRI study, videos containing conspecific faces evoked activity across a broad network that was similar but stronger than the topology that was elicited using scrambled versions of the videos (Schaeffer et al. 2020). They proposed that the lateral prefrontal patches they observed, with activation peaks in areas 45 and 47, were likely face selective, while the activation extending into 8aV may have been more related to saccades made by the animals while viewing the videos. In our study, we found that areas in which neurons with face-selective responses were found overlapped with areas that are saccade-related, with neurons being both visual and saccade-related. Altogether, at the single-neuron level, we observed more widespread responses in the IPFC of marmosets than previously observed in fMRI studies. This may be in part due to the signal specificity of the techniques used. In electrophysiology, only electrically active neurons within the vicinity of the electrodes will be recorded, whereas in fMRI, the blood-oxygen-level-dependent (BOLD) signal reflects localized changes in a much larger area (in terms of spatial resolution). As

a result, the average response of the BOLD signal may be drowning out individual neurons' responses to faces (and other stimuli). On the other hand, here in this study, with electrophysiology, we can detect and report individual neurons' responses to different stimuli. It is important to note that the arrays in the present study did not cover area 45, an area also known to be important for both visual and auditory identification of individuals (Romanski 2007).

We also observed robust auditory responses in IPFC neurons when marmosets were presented with sets of acoustic stimuli. Neurons with auditory responses were found throughout all IPFC subregions sampled, with the highest proportions present in areas 8aD, 9, 46D, and the dorsomedial portion of area 10. In a prior study exploring auditory responses in the marmoset lPFC, neurons that were responsive to long-distance "phee" calls were identified in areas 8aV, 8aD, and 45 (Jovanovic et al. 2022). Our findings suggest a broader distribution of auditory responses across IPFC subregions, potentially due to the presentation of multiple types of calls. However, it's noteworthy that even the solitary presentation of phee calls has been associated with increased cFos expression spanning a considerable expanse of the ventral and posterior PFC (Miller et al. 2010). We observed that neurons selective for at least one type of call were present throughout all IPFC subregions where auditory responses occurred. This finding is similar to those in macaques, in which auditory-responsive cells are found in the vlPFC (area 45, area 47—also known as area 12 of other nomenclature; Romanski and Goldman-Rakic 2002; Romanski et al. 2005), areas 8aD and 46 (Bon and Lucchetti 1994; Hackett et al. 1999; Lanzilotto et al. 2013; Germann and Petrides 2020; Napoli et al. 2021).

We additionally investigated the effects of experimental context on responses of PFC neurons to marmoset calls. We found no evidence for cross-context consistency in the responsiveness of neurons, suggesting that PFC neurons may encode various combinations of call type and context rather than selectivity for a particular call type, which is then modulated by the context in which it is encountered. This is broadly consistent with the observed responses of IPFC neurons in macaques performing visual cognitive tasks, in which responses to cues are dependent upon both their identity and the task context in which they are encountered (White and Wise 1999). Our findings mirror those of Jovanovic et al. (2022) who found that neural responses to vocalizations were highly context-specific, suggesting that neural representations of social signals in primate PFC are not static but highly flexible and likely reflect nuances in behavioral contexts (Nummela et al. 2017). Here, we focused solely on the PFC, but the effects of social context on primate neocortical function are more widespread (Sliwa and Freiwald 2017; Ainsworth et al. 2021; Cléry et al. 2021).

In addition to investigating the functional properties of neurons across a suite of IPFC regions, we exploited the advantage of having simultaneously recorded units to investigate the functional connectivity of units within and across PFC regions. We used an approach devised by Kiani et al. (2015) in which dissimilarity indices are computed across array locations from the discharge rates of single units across the entire duration of a recording session. The values of these indices reflect covariations of responses that are independent of task- or stimulus-related responses, are based primarily on fluctuations in correlated noise between groups, and have been proposed to reflect anatomical connectivity between clusters of neurons (Kiani et al. 2015). We additionally projected these values from the recording locations on our array onto the estimated cytoarchitectonic boundaries of the PFC areas as delineated in the atlas of Paxinos et al. (2012). Similar to their findings in macaque, we observed functional clusters of units that

corresponded broadly to the areal subdivisions of the marmoset lPFC, with some subclusters of units within these divisions. This finding is consistent with the known dominance of interareal anatomical connections within IPFC subregions (Reser et al. 2013), the observation of "patchy" connectivity across IPFC columns (Watakabe et al. 2023), and previous anatomical evidence for lateral to medial connectivity differences in area 10 (Burman et al. 2011). Altogether, our data suggest a spatial segregation of anatomically connected neurons within marmoset IPFC that may correspond to anatomically defined lPFC subregions. It should be noted, however, that cytoarchitectural boundaries are notoriously difficult to determine in the relatively undifferentiated IPFC of the marmoset (Reser et al. 2013), so a direct correspondence between dissimilarity values and cytoarchitecture is best interpreted with some caution. Nonetheless, these data do provide evidence of task-independent spatial clustering of neurons in marmoset IPFC.

The quest to understand how anatomical subdivisions of the IPFC relate to sensory, motor, and cognitive functions is a longstanding pursuit in cognitive neurosciences, as outlined by Wilson et al. (2010). This current study leveraged the small size and relatively lissencephalic cortex of the common marmoset to carry out large-scale neurophysiological mapping of lPFC across two animals. Although the arrays between the two animals do not fully cover the same areas, they do, however, cover most of the IPFCs (to note, during surgical implantation of the arrays, we avoided critical vasculature). Future work with additional animals will allow confirmation of the results reported here. Our observations, similar to numerous electrophysiological studies conducted in rhesus macaques, encompass task-based responses, reactions to a wide array of social and nonsocial stimuli across both auditory and visual modalities, and discharge rate variations contingent on the experimental context (refer to Wise 2008 for a review). Generally, these modulations in discharge rates are distributed across multiple prefrontal areas. However, exceptions include more localized face-selective responses in areas 8aD, 10, and 47, and contralateral visual receptive fields and saccade-related responses in area 8aV. This latter region is likely the marmoset homolog of the marmoset FEF (Selvanayagam et al. 2019; Feizpour et al. 2021). This too is consistent with observations in macaques (Kiani et al. 2015). Overall, these similarities in organization to macaque PFC and the distributed nature of many social and nonsocial representations in marmoset PFC provide supporting evidence for the validity of the marmoset model in investigations of cognitive control and social cognition. An intriguing possibility supported by our data here is that, as in humans and macaques, the marmoset PFC as a whole is a crucial part of a multidemand system engaged to deal with diverse cognitive demands (Duncan 2010), of which social interactions and vocal communication would be a major part. As has been noted previously, these situations require the integration of diverse sources of visual, auditory, and contextbased information and the evaluation of outcomes in the service of behavioral goals (Jovanovic et al. 2022; Samandra et al. 2022; Grijseels et al. 2023). More naturalistic studies combining social interactions and vocal communication with neural recordings, so uniquely suited to the marmoset model, have the potential to advance our understanding of both PFC function in general and its specific role in social cognition.

Limitations

A limitation of this study that must be noted is the variability in electrode array coverage between the two animals, which impacts directly the ability to draw comparisons across brain regions.

While areas 10, 46D, and 46V were substantially overlapped across both marmosets A and B, the coverage of area 8aD was notably absent in marmoset A. As shown in Fig. 3, the number of units modulated during task phases in areas 46V (marmoset A) and 46D (marmoset B) was also relatively low. However, in area 10, which had consistent coverage between the two animals, we observed reliable modulation of units across all task phases.

Given these coverage differences, our capacity to directly compare the two animals is somewhat limited. Therefore, the conclusions regarding task-phase modulation in areas with limited overlap, such as 46V and 46D, should be interpreted with caution. In contrast, findings from area 10, where there is substantial overlap in coverage, are more robust and provide a clearer understanding of the task-related neural activity in both animals.

Acknowledgments

The authors wish to thank Cheryl Vander Tuin, Whitney Froese, and Hannah Pettypiece for animal preparation and care and Peter Zeman for technical assistance. We would also like to thank David Everling for assistance with touchscreen testing.

Author contributions

R.W. performed experiments, analyzed data, prepared figures, and wrote the manuscript. J.S. performed experiments and assisted in data analysis. K.J. assisted in surgeries and data analysis. S.E. designed experiments and performed surgeries. All authors edited the manuscript and SE approved the final version.

Supplementary material

Supplementary material is available at Cerebral Cortex online.

Funding

This research was supported by the Canadian Institutes of Health Research (CIHR) grant FRN148365 to S.E. and the Canada First Research Excellence Fund to BrainsCAN. R.W. was also supported by the Canada First Research Excellence Fund to BrainsCAN and the Next Generation Networks for Neuroscience (NeuroNex). J.S. was supported by a Natural Sciences and Engineering Research Council (NSERC) Canadian Graduate Scholarship (Doctoral).

Conflict of interest statement: None declared.

References

Ainsworth M, Sallet J, Joly O, Kyriazis D, Kriegeskorte N, Duncan J, Schüffelgen U, Rushworth MFS, Bell AH. Viewing ambiguous social interactions increases functional connectivity between frontal and temporal nodes of the social brain. J Neurosci. 2021:41: 6070-6086. https://doi.org/10.1523/JNEUROSCI.0870-20.2021.

Arnsten AFT, Wang MJ, Paspalas CD. Neuromodulation of thought: flexibilities and vulnerabilities in prefrontal cortical network synapses. Neuron. 2012:76:223-239. https://doi.org/10.1016/j. neuron.2012.08.038.

Avants BB, Tustison NJ, Song G, Cook PA, Klein A, Gee JC. A reproducible evaluation of ANTs similarity metric performance in brain image registration. NeuroImage. 2011:54:2033–2044. https:// doi.org/10.1016/j.neuroimage.2010.09.025.

- Averbeck BB, Lee D. Effects of noise correlations on information encoding and decoding. J Neurophysiol. 2006:95:3633-3644. https:// doi.org/10.1152/jn.00919.2005.
- Barbas H, Pandya DN. Architecture and intrinsic connections of the prefrontal cortex in the rhesus monkey. J Comp Neurol. 1989:286: 353-375. https://doi.org/10.1002/cne.902860306.
- Bichot NP, Schall JD, Thompson KG. Visual feature selectivity in frontal eye fields induced by experience in mature macaques. Nature. 1996:381:697-699. https://doi.org/10.1038/381697a0.
- Blum B, Kulikowski JJ, Carden D, Harwood D. Eye movements induced by electrical stimulation of the frontal eve fields of marmosets and squirrel monkeys. Brain Behav Evol. 1982:21:34-41. https://doi. org/10.1159/000121613.
- Boch RA, Goldberg ME. Participation of prefrontal neurons in the preparation of visually guided eye movements in the rhesus monkey. J Neurophysiol. 1989:61:1064-1084. https://doi.org/10.1152/ jn.1989.61.5.1064.
- Bon L, Lucchetti C. Ear and eye representation in the frontal cortex, area 8b, of the macaque monkey: an electrophysiological study. Exp Brain Res. 1994:102:259-271. https://doi.org/10.1007/ BF00227513.
- Burman KJ, Palmer SM, Gamberini M, Rosa MGP. Cytoarchitectonic subdivisions of the dorsolateral frontal cortex of the marmoset monkey (Callithrix jacchus), and their projections to dorsal visual areas. J Comp Neurol. 2006:495:149-172. https://doi.org/10.1002/
- Burman KJ, Reser DH, Yu H-H, Rosa MGP. Cortical input to the frontal pole of the marmoset monkey. Cereb Cortex. 2011:21:1712-1737. https://doi.org/10.1093/cercor/bhq239.
- Cléry JC, Hori Y, Schaeffer DJ, Menon RS, Everling S. Neural network of social interaction observation in marmosets. elife. 2021:10:e65012. https://doi.org/10.7554/eLife.65012.
- Desimone R, Duncan J. Neural mechanisms of selective visual attention. Annu Rev Neurosci. 1995:18:193-222. https://doi.org/10.1146/ annurev.ne.18.030195.001205.
- Dias R, Robbins TW, Roberts AC. Primate analogue of the Wisconsin card sorting test: effects of excitotoxic lesions of the prefrontal cortex in the marmoset. Behav Neurosci. 1996:110:872-886. https:// doi.org/10.1037/0735-7044.110.5.872.
- Duncan J. The multiple-demand (MD) system of the primate brain: mental programs for intelligent behaviour. Trends Coan Sci. 2010:14:172-179. https://doi.org/10.1016/j.tics.2010.01.004.
- Everling S, DeSouza JFX. Rule-dependent activity for Prosaccades and Antisaccades in the primate prefrontal cortex. J Cogn Neurosci. 2005:17:1483-1496. https://doi.org/10.1162/0898929054985455.
- Feizpour A, Majka P, Chaplin TA, Rowley D, Yu H-H, Zavitz E, Price NSC, Rosa MGP, Hagan MA. Visual responses in the dorsolateral frontal cortex of marmoset monkeys. J Neurophysiol. 2021:125: 296-304. https://doi.org/10.1152/jn.00581.2020.
- Fuster JM, Alexander GE. Neuron activity related to shortterm memory. Science. 1971:173:652-654. https://doi.org/10.1126/ science.173.3997.652.
- Germann J, Petrides M. The ventral part of dorsolateral frontal area 8A regulates visual attentional selection and the dorsal part auditory attentional selection. Neuroscience. 2020:441:209-216. https:// doi.org/10.1016/j.neuroscience.2020.05.057.
- Goldman-Rakic PS. Cellular basis of working memory. Neuron. 1995:14:477-485. https://doi.org/10.1016/0896-6273(95)90304-6.
- Grijseels DM, Prendergast BJ, Gorman JC, Miller CT. The neurobiology of vocal communication in marmosets. Ann N Y Acad Sci. 2023:1528:13-28. https://doi.org/10.1111/nyas.15057.
- Hackett TA, Stepniewska I, Kaas JH. Prefrontal connections of the parabelt auditory cortex in macaque monkeys. Brain Res. 1999:817:45-58. https://doi.org/10.1016/S0006-8993(98)01182-2.

- Haile TM, Bohon KS, Romero MC, Conway BR. Visual stimulus-driven functional organization of macaque prefrontal cortex. NeuroImage. 2019:188:427-444. https://doi.org/10.1016/j.neuroimage. 2018.11.060.
- Hoshi E. Functional specialization within the dorsolateral prefrontal cortex: A review of anatomical and physiological studies of nonhuman primates. Neurol Res. 2006:54:73-84.
- Hung C-C, Yen CC, Ciuchta JL, Papoti D, Bock NA, Leopold DA, Silva AC. Functional MRI of visual responses in the awake, behaving marmoset. NeuroImage. 2015:120:1-11. https://doi.org/10.1016/j. neuroimage.2015.06.090.
- Hwang J, Mitz AR, Murray EA. NIMH MonkeyLogic: Behavioral control and data acquisition in MATLAB. J Neurosci Methods. 2019:323: 13-21. https://doi.org/10.1016/j.jneumeth.2019.05.002.
- Johnston KD, Barker K, Schaeffer L, Schaeffer D, Everling S. Methods for chair restraint and training of the common marmoset on oculomotor tasks. J Neurophysiol. 2018:119:1636-1646. https://doi. org/10.1152/jn.00866.2017.
- Johnston K, Ma L, Schaeffer L, Everling S. Alpha oscillations modulate preparatory activity in marmoset area 8Ad. J Neurosci. 2019:39: 1855-1866. https://doi.org/10.1523/JNEUROSCI.2703-18.2019.
- Jovanovic V, Fishbein AR, de la Mothe L, Lee K-F, Miller CT. Behavioral context affects social signal representations within single primate prefrontal cortex neurons. Neuron. 2022:110:1318-1326.e4. https://doi.org/10.1016/j.neuron.2022.01.020.
- Kiani R, Cueva CJ, Reppas JB, Peixoto D, Ryu SI, Newsome WT. Natural grouping of neural responses reveals spatially segregated clusters in Prearcuate cortex. Neuron. 2015:85:1359-1373. https:// doi.org/10.1016/j.neuron.2015.02.014.
- Kondo T, Saito R, Otaka M, Yoshino-Saito K, Yamanaka A, Yamamori T, Watakabe A, Mizukami H, Schnitzer MJ, Tanaka KF, et al. Calcium transient dynamics of neural ensembles in the primary motor cortex of naturally behaving monkeys. Cell Rep. 2018: 24:2191-2195.e4. https://doi.org/10.1016/j.celrep.2018.07.057.
- Kubota K, Niki H. Prefrontal cortical unit activity and delayed alternation performance in monkeys. J Neurophysiol. 1971:34:337–347. https://doi.org/10.1152/jn.1971.34.3.337.
- Landman R, Sharma J, Hyman JB, Fanucci-Kiss A, Meisner O, Parmar S, Feng G, Desimone R. Close-range vocal interaction in the common marmoset (Callithrix jacchus). PLoS One. 2020:15:e0227392. https://doi.org/10.1371/journal.pone.0227392.
- Lanzilotto M, Perciavalle V, Lucchetti C. Auditory and visual systems organization in Brodmann area 8 for gaze-shift control: where we do not see, we can hear. Front. Behav Neurosci. 2013:7:1–3. https:// doi.org/10.3389/fnbeh.2013.00198.
- Li X, Morgan PS, Ashburner J, Smith J, Rorden C. The first step for neuroimaging data analysis: DICOM to NIfTI conversion. J Neurosci Methods. 2016:264:47–56. https://doi.org/10.1016/ j.jneumeth.2016.03.001.
- Liu C, Ye FQ, Yen CC-C, Newman JD, Glen D, Leopold DA, Silva AC. A digital 3D atlas of the marmoset brain based on multi-modal MRI. NeuroImage. 2018:169:106-116. https://doi. org/10.1016/j.neuroimage.2017.12.004.
- Liu C, Yen CC-C, Szczupak D, Ye FQ, Leopold DA, Silva AC. Anatomical and functional investigation of the marmoset default mode network. Nat Commun. 2019:10:1975. https://doi.org/10.1038/ s41467-019-09813-7.
- Mansouri FA, Buckley MJ, Mahboubi M, Tanaka K. Behavioral consequences of selective damage to frontal pole and posterior cingulate cortices. Proc Natl Acad Sci USA. 2015:112:E3940-E3949. https://doi.org/10.1073/pnas.1422629112.
- Mansouri FA, Koechlin E, Rosa MGP, Buckley MJ. Managing competing goals — a key role for the frontopolar cortex. Nat Rev Neurosci. 2017:18:645-657. https://doi.org/10.1038/nrn.2017.111.

- Miller EK, Cohen JD. An integrative theory of prefrontal cortex function. Annu Rev Neurosci. 2001:24:167-202. https://doi.org/10.1146/ annurev.neuro.24.1.167.
- Miller CT, DiMauro A, Pistorio A, Hendry S, Wang X. Vocalization induced CFos expression in marmoset cortex. Front Integr Neurosci. 2010:4:125, 1-15. https://doi.org/10.3389/fnint.2010.00
- Miller CT, Freiwald WA, Leopold DA, Mitchell JF, Silva AC, Wang X. Marmosets: a neuroscientific model of human social behavior. Neuron. 2016:90:219-233. https://doi.org/10.1016/j.neuron.
- Mitchell JF, Leopold DA. The marmoset monkey as a model for visual neuroscience. Neurosci Res. 2015:93:20-46. https://doi. org/10.1016/j.neures.2015.01.008.
- Napoli JL, Camalier CR, Brown A-L, Jacobs J, Mishkin MM, Averbeck BB. Correlates of auditory decision-making in prefrontal, auditory, and basal lateral amygdala cortical areas. J Neurosci. 2021:41:1301-1316. https://doi.org/10.1523/JNEUROSCI.2217-20. 2020.
- Nummela SU, Jovanovic V, de la Mothe L, Miller CT. Social contextdependent activity in marmoset frontal cortex populations during natural conversations. J Neurosci. 2017:37:7036-7047. https:// doi.org/10.1523/JNEUROSCI.0702-17.2017.
- O'Reilly RC. The what and how of prefrontal cortical organization. Trends Neurosci. 2010:33:355-361. https://doi.org/10.1016/j. tins.2010.05.002.
- Okano H. Current status of and perspectives on the application of marmosets in neurobiology. Annu Rev Neurosci. 2021:44:27-48. https://doi.org/10.1146/annurev-neuro-030520-101844.
- Paxinos G, Watson C, Petrides M, Rosa M, Tokuno H. The marmoset brain in stereotaxic coordinates. London; Waltham, MA: Academic Press: 2012.
- Peterson J, Chaddock R, Dalrymple B, Van Sas F, Gilbert KM, Klassen LM, Gati JS, Handler WB, Chronik BA. Development of a gradient and shim insert system for marmoset imaging at 9.4 T. Paper Presented at 26th Annual Meeting of International Society for Magnetic Resonance in Medicine, Paris. June 2018.
- Petrides M. Lateral prefrontal cortex: architectonic and functional organization. Philos Trans R Soc B. 2005:360:781-795. https://doi. org/10.1098/rstb.2005.1631.
- Rao SC, Rainer G, Miller EK. Integration of what and where in the primate prefrontal cortex. Science. 1997:276:821-824. https://doi. org/10.1126/science.276.5313.821.
- Reser DH, Burman KJ, Yu H-H, Chaplin TA, Richardson KE, Worthy KH, Rosa MGP. Contrasting patterns of cortical input to architectural subdivisions of the area 8 complex: a retrograde tracing study in marmoset monkeys. Cereb Cortex. 2013:23:1901-1922. https://doi.org/10.1093/cercor/bhs177.
- Riley MR, Qi X-L, Constantinidis C. Functional specialization of areas along the anterior–posterior axis of the primate prefrontal cortex. Cereb Cortex. 2016:27:3683-3697. https://doi.org/10.1093/cercor/ hhw190
- Romanski LM. Representation and integration of auditory and visual stimuli in the primate ventral lateral prefrontal cortex. Cereb Cortex. 2007:17:i61-i69. https://doi.org/10.1093/cercor/
- Romanski LM, Averbeck BB. The primate cortical auditory system and neural representation of conspecific vocalizations. Annu Rev Neurosci. 2009:32:315-346. https://doi.org/10.1146/annurev. neuro.051508.135431.
- Romanski LM, Goldman-Rakic PS. An auditory domain in primate prefrontal cortex. Nat Neurosci. 2002:5:15-16. https://doi. org/10.1038/nn781.

- Romanski LM, Averbeck BB, Diltz M. Neural representation of vocalizations in the primate ventrolateral prefrontal cortex. J Neurophysiol. 2005:93:734-747. https://doi.org/10.1152/jn.00675.2004.
- Rossi AF, Pessoa L, Desimone R, Ungerleider LG. The prefrontal cortex and the executive control of attention. Exp Brain Res. 2009:192: 489-497. https://doi.org/10.1007/s00221-008-1642-z.
- Sadakane O, Masamizu Y, Watakabe A, Terada S-I, Ohtsuka M, Takaji M, Mizukami H, Ozawa K, Kawasaki H, Matsuzaki M, et al. Longterm two-photon calcium imaging of neuronal populations with subcellular resolution in adult non-human primates. Cell Rep. 2015:13:1989–1999. https://doi.org/10.1016/j.celrep.2015.10.050.
- Sallet J, Mars RB, Noonan MP, Neubert F-X, Jbabdi S, O'Reilly JX, Filippini N, Thomas AG, Rushworth MF. The Organization of Dorsal Frontal Cortex in humans and macaques. J Neurosci. 2013:33: 12255-12274. https://doi.org/10.1523/JNEUROSCI.5108-12.2013.
- Samandra R, Haque ZZ, Rosa MGP, Mansouri FA. The marmoset as a model for investigating the neural basis of social cognition in health and disease. Neurosci Biobehav Rev. 2022:138:104692. https://doi.org/10.1016/j.neubiorev.2022.104692.
- O Scalaidhe SP, Wilson FA, Goldman-Rakic PS. Face-selective neurons during passive viewing and working memory performance of rhesus monkeys: evidence for intrinsic specialization of neuronal coding. Cereb Cortex. 1999:9:459-475. https://doi. org/10.1093/cercor/9.5.459.
- Schaeffer DJ, Gilbert KM, Gati JS, Menon RS, Everling S. Intrinsic functional boundaries of lateral frontal cortex in the common marmoset monkey. J Neurosci. 2019a:39:1020-1029. https://doi. org/10.1523/JNEUROSCI.2595-18.2018.
- Schaeffer DJ, Gilbert KM, Hori Y, Hayrynen LK, Johnston KD, Gati JS, Menon RS, Everling S. Task-based fMRI of a freeviewing visuo-saccadic network in the marmoset monkey. NeuroImage. 2019b:202:116147. https://doi.org/10.1016/j.neuroimage. 2019.116147.
- Schaeffer DJ, Selvanayagam J, Johnston KD, Menon RS, Freiwald WA, Everling S. Face selective patches in marmoset frontal cortex. Nat Commun. 2020:11:4856. https://doi.org/10.1038/s41467-020-
- Selvanayagam J, Johnston KD, Schaeffer DJ, Hayrynen LK, Everling S. Functional localization of the frontal eye fields in the common marmoset using microstimulation. J Neurosci. 2019:39:9197-9206. https://doi.org/10.1523/JNEUROSCI.1786-19.2019.
- Sliwa J, Freiwald WA. A dedicated network for social interaction processing in the primate brain. Science. 2017:356:745-749. https:// doi.org/10.1126/science.aam6383.
- Sugihara T, Diltz MD, Averbeck BB, Romanski LM. Integration of auditory and visual communication information in the primate ventrolateral prefrontal cortex. J Neurosci. 2006:26:11138-11147. https://doi.org/10.1523/JNEUROSCI.3550-06.2006.
- Thompson KG, Hanes DP, Bichot NP, Schall JD. Perceptual and motor processing stages identified in the activity of macaque frontal eye field neurons during visual search. J Neurophysiol. 1996:76: 4040-4055. https://doi.org/10.1152/jn.1996.76.6.4040.
- Tsujimoto S, Genovesio A, Wise SP. Evaluating self-generated decisions in frontal pole cortex of monkeys. Nat Neurosci. 2010:13: 120-126. https://doi.org/10.1038/nn.2453.
- Tsujimoto S, Genovesio A, Wise SP. Neuronal activity during a cued strategy task: comparison of dorsolateral, orbital, and polar prefrontal cortex. J Neurosci. 2012:32:11017-11031. https://doi. org/10.1523/JNEUROSCI.1230-12.2012.
- Van Essen DC, Glasser MF. Parcellating cerebral cortex: how invasive animal studies inform noninvasive mapmaking in humans. Neuron. 2018:99:640-663. https://doi.org/10.1016/j.neuron.2018. 07.002.

- Wallis JD, Anderson KC, Miller EK. Single neurons in prefrontal cortex encode abstract rules. Nature. 2001:411:953-956. https:// doi.org/10.1038/35082081.
- Watakabe A, Skibbe H, Nakae K, Abe H, Ichinohe N, Rachmadi MF, Wang J, Takaji M, Mizukami H, Woodward A, et al. Local and long-distance organization of prefrontal cortex circuits in the marmoset brain. Neuron. 2023:111:2258-2273.e10. https://doi. org/10.1016/j.neuron.2023.04.028.
- White IM, Wise SP. Rule-dependent neuronal activity in the prefrontal cortex. Exp Brain Res. 1999:126:315-335. https://doi. org/10.1007/s002210050740.
- Wilson CRE, Gaffan D, Browning PGF, Baxter MG. Functional localization within the prefrontal cortex: missing the forest for the trees? Trends Neurosci. 2010:33:533-540. https://doi.org/10.1016/j. tins.2010.08.001.
- Wise SP. Forward frontal fields: phylogeny and fundamental function. Trends Neurosci. 2008:31:599-608. https://doi.org/10.1016/j. tins.2008.08.008.
- Wong RK, Selvanayagam J, Johnston KD, Everling S. Delay-related activity in marmoset prefrontal cortex. Cereb Cortex. 2023:33:3523-3537. https://doi.org/10.1093/cercor/bhac